Habitable Planet, 2026, 2(1), 170–189

Scilight

Habitable Planet

Journal Homepage: https://www.sciltp.com/journals/hp

Review

Urban Expansion and Agricultural Land Conflict in Southern Brazil: Implications for Sustainable Land Use Policy

Guilherme Peterle Schmitz [1], Emanuelle Goellner [2], Brian William Bodah [3,4], Marcos Roberto dos Santos [1], Giana Mores [1], Grace Tibério Cardoso [1], Richard Thomas Lermen [1] and Alcindo Neckel [1,2,*]

[1] Atitus Educação, Passo Fundo 99070-220, RS, Brazil
[2] University of Minho, 4710-057 Guimarães, Portugal
[3] Thaines and Bodah Center for Education and Development, Selah, WA 98942, USA
[4] Yakima Valley College, Yakima, WA 98902, USA
[*] Correspondence: alcindo.neckel@atitus.edu.br

ABSTRACT

This study adopts an integrated simulation framework based on Cellular Automata and Artificial Neural Networks (CA-ANN) to model land use and land cover (LULC) transitions driven by urban expansion. By combining machine learning with spatial modeling, the approach enables the forecasting of urban growth dynamics and supports data-driven urban planning. The objective is to assess urban sprawl in the city of Passo Fundo, southern Brazil, using LULC change simulations from 2002 to 2043. Satellite imagery from 2002 to 2023 indicate for supervised classification of three land cover classes—urbanized areas, forests, and non-urbanized areas—alongside key spatial variables, including hypsometry, proximity to water bodies, railways, central business districts, and road networks. These variables served as inputs to the CA-ANN model to simulate future land use scenarios for 2033 and 2043. Results indicate a 45% increase in urbanized areas from 2002 to 2023, with projections reaching 66% growth by 2043, absolute land area expansion. This urban expansion primarily occurs at the expense of agricultural and forest areas, underscoring the risks of landscape fragmentation, biodiversity loss, and pressure on agricultural lands. The findings highlight the urgency of integrating spatial intelligence into sustainable land governance strategies, particularly in regions where urbanization intersects with agribusiness territories and food security systems.

ARTICLE INFO

History:

Received: 29 November 2025
Revised: 06 January 2026
Accepted: 16 January 2026
Published: 26 January 2026

Keywords:

Urban sprawl;
Land Use Simulation;
Land use and land cover change;
Public policy;
Sustainability management;
Global south

Citation:

Schmitz, G.P.; Goellner, E.; Bodah, B.W.; et al. Urban Expansion and Agricultural Land Conflict in Southern Brazil: Implications for Sustainable Land Use Policy. *Habitable Planet* **2026**, *2*(1), 170–189. https://doi.org/10.63335/j.hp.2026.0033

Research Highlights

- Forecasting of urban growth dynamics and supports data-driven urban planning.
- Results show 45% increase in urbanized areas from 2002 to 2023.
- Risks of landscape fragmentation, biodiversity loss, and pressure on agricultural lands.

1. Introduction

The urban expansion of global cities and changes in land use require the creation and implementation of new public policies to support future projects focused on environmental quality in the built environment [1, 2]. For González-Calle [3], urban expansion results from phenomena driven by contemporary societies, arising from social, environmental, and economic transformations in cities worldwide.

Inadequate urban expansion that prioritizes environmental quality can lead to various problems for the city, including an increased risk of floods [4, 5]. This occurs because urban expansion, according to Almulhim and Cobbinah [6], is often conceived without adequate planning, disregarding negative environmental impacts and the lack of infrastructure appropriate to the city's needs. These negative impacts on urban land use are exacerbated by the constant removal of trees and constructions located in irregular areas, which contribute to the worsening of environmental problems, causing social, environmental, and economic damage attributed to the population's quality of life [7, 8].

Dehghani et al. [9] and Ogara et al. [10] highlight that environmental problems arising from inadequate urban expansion reveal a lack of projects aimed at the continuous sustainable development of urban areas, capable of promoting solutions to mitigate adverse impacts, and that this will define future decision-making by government agents. Consequently, for consolidating public policies that support more effective urban projects, knowledge of the built environment's characteristics is necessary [11, 12].

To facilitate these studies, remote sensing presents itself as an efficient tool for understanding the physical characteristics of the built environment at different scales, through the use of geotechnologies obtained via satellite imagery, making it possible to get precise information about the characteristics of the urban landscape [13, 14]. The scientific evolution of the applicability of geotechnologies enables the obtaining of geospatial detection and analysis results, capable of achieving detailed information on land use and land cover throughout the process of urban expansion, represented by computational simulation using machine learning algorithms with a model based on cellular automata and artificial neural networks (CA-ANN) [15, 16].

Regarding the development of the artificial neural network (ANN), the algorithm is based, according to Onsay et al. [17] and Shukla et al. [18], on the functioning of the human brain, where interconnected artificial neurons perform weighted sum operations applied to input data, being subjected to non-linear activation functions. For Adhab et al. [19], the use of ANN allows the adjustment of weights between data connections by simulated neurons, aiming to mitigate errors in predicted outputs and to learn and extract complex characteristics from the data. In this context, the ANN algorithm has proven to be a promising approach in land use and land cover simulation, due to its ability to process a wide variety of input data, identifying patterns of change in land use and land cover, enabling greater accuracy in quantitative computational simulations, and potentially integrating a cellular automata (CA) algorithm for spatially based output [18–20].

Cellular automation (CA) models require the determination of weights to ensure proper functioning, with the ability to change state at predefined iterations, regulated by neighborhood conditions [20, 21]. Based on the cellular automata and artificial neural network (CA-ANN) instrument, the model allows the CA weights to be configured through machine learning to predict changes in land use and land cover from the results of the ANN training process, which occurs through land use and land cover (LULC) base maps and their relationship with other variables, aiming at understanding the patterns of change in land use and land cover in a given space-time [19, 22, 23]. These predictive data generated from CA-ANN can be analyzed spatially and quantitatively using geoprocessing techniques, enabling more assertive urban projects [19, 23, 24].

The use of the CA-ANN method is justified by the applicability of new technologies in the built environment to mitigate problems arising from urban expansion [25, 26]. Consequently, a study on urban expansion with the application of CA-ANN instruments presents contributions to the viability of this method, assisting the designer in the development of urban projects, revealing potential for understanding and analyzing urban expansion in different cities around the world [27, 28]. Furthermore, this study contributes to new global discussions, using the city of Passo Fundo, located in southern Brazil, as a case study. Passo Fundo stands out for its importance within the region, with the highest growth performance in the public and private services sector, quantified at 40.4% [29].

The scientific contributions of this study promote more efficient urban projects aligned with future urban expansion, potentially benefiting government agents in the

construction of spaces that provide a higher quality of life for the population, while preserving the urban landscape, as indicated by other studies on a global scale [30–32].

Given this backdrop, this study aims to analyze future urban expansion in the city of Passo Fundo through the simulation of land use and land cover change (LULC) using a cellular automata-artificial neural network (CA-ANN) model. With the interpretation of future urban expansion carried out in this study, it is expected to support the development of projects that incorporate the relationship between the future expansion of cities, enabling the replication of the method in different urban contexts around the world, contributing to mitigating the problems associated with urban expansion, to achieve a higher quality of life for the world's population.

2. Materials and Methods

2.1. Study Area and Methodological Definition of the Variables Used

The study area is located in the city of Passo Fundo, in the north of Rio Grande do Sul (RS), in the southern region of Brazil, where 214,811 inhabitants were concentrated in 2025. The city's area is 784.406 km^2, totaling a population density of 262.89 inhabitants/km^2 [29]. It is considered a regional capital due to its high economic and service influence, both direct and indirect, in southern Brazil [29].

Regarding the variables used in this study, they were organized into distinct groups, as recommended by Pan et al. [33], Rifat and Liu [34], and Zheng et al. [35], where it became possible to structure them with the definition of three categories: (A) Landscape factors, which correspond to the main variables related to LULC and which form the basis to be used in the simulations; (B) Resistance factors, which represent variables capable of limiting or hindering the expansion of urbanized areas; and (C) Driving factors, consisting of urban elements that act as vectors and stimuli for horizontal expansion, driving urban growth [33–35]. Zheng et al. [35], Kuhn [36], and Parsch et al. [37] justify the use of urbanized, forested, and non-urbanized classes, as they are essential for understanding urban expansion in cities, thereby supporting the selection of these variables for this study.

Table 1 presents the representation of the three defined groupings, with Landscape Factors (A) comprising the variables that represent the main elements of LULC within the Passo Fundo area. The variables categorized in the landscape factors address the identified elements, according to Zheng et al. [35], Kuhn [36], and Parsch et al. [37] define them as: (1) Urbanized area—any built-up area, pavement, or exposed soil intended for civil construction, located near the city's urban perimeter; (2) Forests—Any wooded area in the city; (3) Non-urbanized area—Any other element that is not part of wooded areas or urbanized areas, being mostly areas intended for agriculture, livestock, or exposed soil, in addition to containing other minor characteristics of open fields, buildings and rural communities, small bodies of water, roads, and some quarries. The Resistance Factors group (B) includes the variables: (4) Hypsometry, which represents the relationship with topography; and (5) Proximity to Water bodies, which relates to the proximity to the various bodies of water present in the city. The Direction Factors group (C) deals with the variables: (6) Proximity to Railways; (7) Proximity to the Urban center; (8) Proximity to Main roads; and (9) Proximity to Secondary roads [35–37].

Landscape factors (A) were represented by land use and land cover maps [37]. Along with the group of resistance factors (B), characterized by the representation of varied maps containing the following information: topography represented by hypsometric maps; and water bodies by proximity maps [35, 38]. For the variables in the driving factors group (C), proximity maps were used to provide a more comprehensive representation, based on the studies of Pan et al. [33] and Rifat and Liu [34], which used similar mapping models to represent and quantify the variables.

Table 1. Definitions of groupings, variables, mapping models and collection date.

Groups	Variables	Mapping Models	Collection Date
(A) Landscape factors	(1) Urbanized area (2) Forests (3) Non-urbanized area	Land use and land cover maps	2002, 2007, 2013, 2018 and 2023
(B) Resistance factors	(4) Hypsometry (5) Water bodies	Hypsometric map	2023
(C) Driving factors	(6) Railways (7) Urban center (8) Main roads	Proximity maps	
	(9) Secondary roads	Proximity maps	2002, 2007, 2013, 2018 and 2023

The years for collecting the variables followed a regular five-year interval, adopting a retrospective approach that began in 2023, as it was the most recent year available during the research. Data collection then went back to 2002, the furthest possible date given the Landsat 7 and Landsat 8 images, selected for their more recent sensor technologies and 30-m spatial resolution, which ensures data comparability and consistency within the established time frame. The LULC maps (1, 2, and 3) and the Secondary roads variable (9) followed this five-year interval, due to the significant changes observed over the period, aligning with the methodology adopted in benchmark studies on a global scale [39–41]. The other variables (4, 5, 6, 7, and 8) were observed within the same period, but only 2023 was collected, as none showed variation during the analyzed period.

2.2. Methodological Procedures Applied to the Mapped Variables

The process of mapping the variables was based on Geographic Information System (GIS), involving the graphical and quantitative representation of variables, in a georeferenced and standardized way for all cartography. These maps were created in QGIS 3.16.7 using raster layers with a 30 m $\times$ 30 m resolution in the SIRGAS 2000-UTM zone 22S (EPSG:31982) CRS, covering the geographic region of Passo Fundo [29]. LULC maps were created in raster format from Landsat 7 satellite imagery, launched in 1999, which enabled data collection for 2002 and 2007, and from Landsat 8, launched in 2013, which was responsible for data collection for 2013, 2018, and 2023. All images were obtained from the United States Geological Survey (USGS) via the Earth Explorer platform [42].

Based on Landsat image color composites, a supervised classification algorithm was applied in QGIS 3.16.7 using the Dzetsaka plugin [43]. This enabled automatic classification of the entire city of Passo Fundo into previously defined classes: urbanized area, forests, and non-urbanized area. This process resulted in five base raster maps at 30 m $\times$ 30 m resolution, representing land use and land cover for 2002, 2007, 2013, 2018, and 2023. Subsequently, the tool, native to QGIS, indicate to smooth the areas generated by the supervised classification and make them more consistent, as recommended by Aszkowski et al. [44] and Jakimow et al. [45]. Each LULC class was assigned a specific color, as per Mafiana et al. [46] and Rodríguez-Ortega et al. [47], with the following contrasting colors used for the three classes to facilitate visualization: red for urbanized areas; green for forests; and yellow for non-urbanized areas.

The hypsometry variable was represented using a hypsometric map, constructed according to specific steps for topographic representation. Using Digital Elevation Model (DEM) data provided by the USGS [42], the base of the hypsometric map was generated. In QGIS 3.16.7 with GRASS 7.8.5, altimetric variations in the city of Passo Fundo were classified into the following ranges: 475–530 m, 530–580 m, 580–630 m, 630–680 m, 680–725 m, and above 725 m. For the graphic representation, the "Topography" color palette was adopted, commonly used to illustrate topographic surveys [46, 47].

Proximity maps represent the distance to the vector elements of the analyzed variables: in the Resistance Factors group, proximity to water bodies; and, in the Direction Factors group, proximity to railways, urban centers, main roads, and secondary roads. In short, these maps indicate radial distances from the reference elements, so that as distance increases, the raster layer values increase, and conversely, decrease in areas close to the analyzed elements [33, 34].

These maps were created in QGIS 3.16.7 using vector data from IBGE [29]. After all vector layers were added, they were transformed into raster layers using the native QGIS tool (rasterize) at a resolution of 30 m $\times$ 30 m, unit in geographic coordinates and byte output type, where the overlap of vectors with the raster being generated is transformed into pixels with a value of 1, zeroing the pixel values that are not being overlapped by vectors. Finally, the output raster layer is inserted into the native QGIS tool "proximity (raster distance)" [43], where radial distances for the variables were calculated, maintaining the quartile classification standard provided by the software. For graphical representation, a color palette was defined from red to blue, where red indicates proximity to the variable and blue indicates greater distance from the element [46, 47].

With all the maps generated, the rasters were standardized using the native raster standardization tool of the QGIS 3.16.7 software, which allowed for the rectification of the raster mesh pixels, in addition to standardizing all maps in the same coordinate reference system (CRS) and the same pixel size [48, 49]. Consequently, all maps used in this study were standardized within the SIRGAS 2000-UTM zone 22S CRS (EPSG:31982), with a pixel size of 30 m $\times$ 30 m and a total dimension for all rasters of X: 1517, Y: 1077.

2.3. LULC Simulation Procedures with the MOLUSCE Plugin

The mapping of the stipulated variables and the standardization of the maps produced in this study began with integrating the data into the CA-ANN model using the Modules for Land Use Change Simulations (MOLUSCE) plugin within QGIS 2.16.3. According to Kafy et al. [5] and Julien et al. [50], it is necessary to include LULC variables for the analyzed period, in chronological sequence, using an initial and a final LULC map as the basis for the simulation. These maps were calculated in conjunction with the other variables defined previously (hypsometry, proximity to water bodies, proximity to railways, proximity to the urban center, proximity to main roads, and proximity to secondary roads), based on the methodological application of other similar studies on a global scale [5, 50, 51].

All generated maps were imported into the MOLUSCE plugin and subjected to geometry checking, ensuring that the dimensions were aligned correctly with the standardization [5]. After inserting all variables, the MOLUSCE plugin provides information for manual checking of quantita-

tive statistical data, generating tables that show the number of areas in LULC classes during the analyzed spatiotemporal interval, the transition matrix between LULC classes, and the Pearson correlation table [5, 52].

The transition matrix enables a more precise analysis of changes in LULC classes within the predetermined initial and final spatiotemporal intervals [52, 53]. This transition matrix demonstrates the frequency or probability with which a given land use and land cover class is converted into another class, allowing the identification of patterns and trends in LULC transformations [52, 53]. High values (close to 1) in a cell indicate a high conversion rate between classes, while low values (close to 0) suggest less frequent changes. The diagonal of the matrix identifies the variables that remained in the same class over time, thereby assessing the stability of land use and land cover categories [5, 50, 51].

Regarding Pearson's correlation coefficient, it shows a variation from -1 to 1, providing a quantitative measure of the relationship between two variables, where values close to 1 indicate a strong positive correlation, suggesting that as one variable increases in value, the other tends to increase [52–54]. On the other hand, values close to -1 indicate a strong negative correlation, suggesting that an increase in one variable is associated with a decrease in another variable [52, 54]. Values close to 0 indicate little or no correlation, suggesting no clear linear relationship between the variables [53, 54].

In this study, an Artificial Neural Network with a Multilayer Perceptron (ANN-MLP) architecture indicate. According to Khalid et al. [20], Khan and Sudheer [55], and Shomope et al. [56], the ANN-MLP is a mathematical model that interprets hidden urban growth patterns based on the variables provided, enabling it to generalize and predict from hidden data. The algorithm's weight calibration process is guided by the projection efficiency achieved in each simulation attempt (iteration) during the machine learning stage, taking into account the patterns of change in LULC, according to the LULC maps (2002, 2007, 2013, 2018, and 2023) inserted in the start and end year layers (dependent variable), in addition to the variables that make up the groups of resistance factors and driving factors (independent variables) used by the same algorithm to formulate the logic of the patterns of change in LULC (transition potential) that is used as input for cellular automata in the classification of future LULC, as determined by Khalid et al. [20], Khan and Sudheer [55], in the methodological procedures of their research.

Parameters related to the transition potential were defined, which directly alter the result of ANN training, as shown by Khalid et al. [20], Khan and Sudheer [55], and Shomope et al. [56]: (1) "number of samples", which refers to the number of samples used to train the model; (2) "neighbourhood", which defines the size of the neighborhood by calculating the influence of pixels adjacent to the sampled pixel; (3) "learning rate", which controls the speed at which the model adjusts its weights during training; (4) "maximum iterations", which defines the number of iterations for training, influencing the number of times the model will process the data; (5) "hidden layers", which specifies the number of hidden layers in the artificial neural network; and (6) "Momentum", which accelerates the model's trend, preventing oscillations during training in an adjusted transition of the ANN weights.

After the transition potential calculation stage, predictive urban expansion scenarios were developed using cellular automata (CA). The CA integrated into the MOLUSCE plugin can be defined as a stochastic cellular automaton model based on a Markov chain, which evaluates the current state of the sampled pixel using adjacent pixels and calculates neighborhood randomness in conjunction with the transition potential. This transforms the patterns of the hidden datasets from the ANN processing stage into new simulations of future land use and land cover scenarios [16, 20]. It is worth noting that, in this study, the CA-ANN consists of a structure trained using historical data organized into distinct calibration and validation periods related to the analyzed timeframe from 2002 to 2043. The data generated for the period from 2002 to 2043 were used in the calibration phase, which refers to model training for independent validation. This approach, according to Onsay et al. [17] and Shukla et al. [18], allows the assessment of the model's generalization capability, in addition to reducing risks that could compromise model performance, thereby ensuring high robustness in the estimates obtained in the final results.

In the CA-ANN model, the iteration number parameter objectively determines the time interval of the simulated future scenario. When this value is 1, the simulation is calculated, representing a future scenario that advances by several years, equivalent to the period defined between the initial and final LULC maps; if defined as 2, it will be comparable to twice this period, and so on [20, 55]. In this study, the value 1 was always used as the iteration number parameter to generate each scenario, varying only the periods of the input LULC maps (initial and final), according to the period allocated to each simulation within the scenarios presented in the results section [16].

The MOLUSCE tool provides a means to validate results by comparing the simulated LULC map with another LULC map from the same date, created from satellite imagery [57, 58]. The application of this validation yielded the correlation percentage (which assesses map similarity) and the Kappa index for each simulated scenario. According to Foody [59], Ismaeel and Kumar [60] state that the Kappa index ranges from 0 to 1, where: a Kappa value greater than 0.80 indicates strong agreement and accuracy of the simulation; a Kappa index between 0.40 and 0.80 reflects intermediate accuracy of the simulation; and a Kappa value less than 0.40 reveals a low correlation between the simulated scenario and the LULC map created from satellite imagery [59–61].

Figure 1 illustrates the logical process for quality control of results during CA-ANN model calibration and testing in the application, using the MOLUSCE plugin. When performing the simulation method, it begins with the definition of the LULC variables (2002, 2007, 2013, 2018 and 2023), according to the methodological standards of Blissag et al. [57] and Ali et al. [58], where the allocation of the other variables that make up the groups of resistance factors and direction factors (hypsometry, proximity to water bodies, proximity to railways, proximity to the urban center, proximity to main roads and proximity to secondary roads) was considered; calibration of the ANN and the definition of its parameters (number of samples; neighborhood; learning rate; maximum iterations; hidden layers; and momentum); the generation of the transition potential by the ANN; the configuration of the CA, with the simulation iteration parameter; and the final stage of validating the generated simulation.

When validation did not yield satisfactory results, the ANN parameters were reviewed and adjusted until better performance was achieved [20, 55, 56]. After obtaining results deemed adequate by the ANN methodology, according to Shomope et al. [56], Tola and Deyassa [61], the simulated maps were analyzed in detail to identify potential errors or inconsistencies. If the projected scenario did not conform to the LULC maps derived from satellite images—or presented insufficient correlation and Kappa index values—the process was repeated, with the redefinition of the ANN parameters [20, 55, 56].

When the simulation was adequate, the results (maps, parameters, tables, and graphs) were exported and stored [56, 59], to enhance the reliability of the data acquired in this research. This cycle of validation, adjustment, and analysis was essential to ensure the statistical quality of the simulations before determining the final results. The model parameter specification that yielded the most reliable simulations indicate to project future LULC scenarios for 2033 and 2043, thereby ensuring greater reliability relative to the data obtained in the simulations validated in this study.

3. Results and Discussion

3.1. Mapping Applied to Landscape Factors

The mapping of variables within the landscape factor grouping was represented by land-use and land-cover maps. Figure 2 shows the constant changes in both LULC classes that characterize the area within the limits of Passo Fundo/RS, Brazil. The urbanized area class shows continuous expansion, while the other courses exhibit fewer variations over the analyzed time periods. Regarding the urbanized area (red scale), it represents the consolidated urban fabric and its expansion over the analyzed period from 2002 to 2023, together with forested areas (green scale), which include areas with denser arboreal vegetation cover, and non-urbanized areas (yellow scale), which encompass agricultural lands, fields, pastures, and exposed soils (Figure 2).

When this information was analyzed in conjunction with Table 2, it was complemented by trends in temporal landscape transformation, which related the interactions analyzed across the entire study area. According to Zhang et al. [62] and Dinh et al. [63], studying landscape interactions is necessary for understanding land use. It has become increasingly significant over the years, requiring government action to create future public policies that will contribute to the environmental, social, and economic reorganization of cities. These data related to urban expansion can motivate the development of new public policies, enabling the consolidation of actions by governmental agents in urban governance [62, 63].

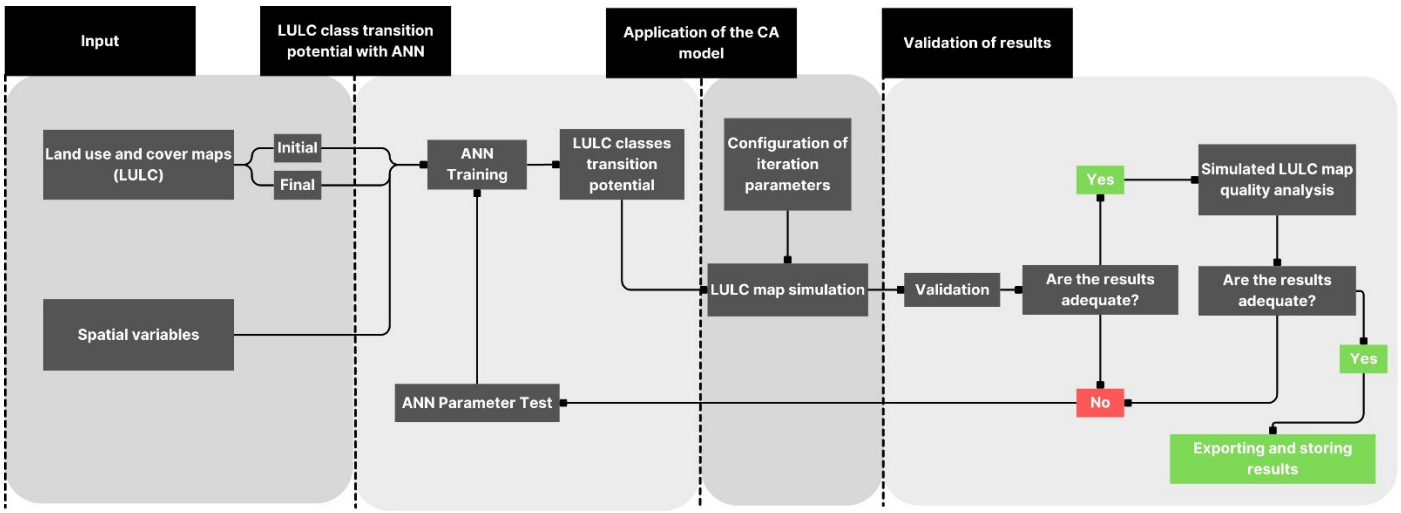

Figure 1. Flowchart of the testing phase of the LULC simulation using CA-ANN.

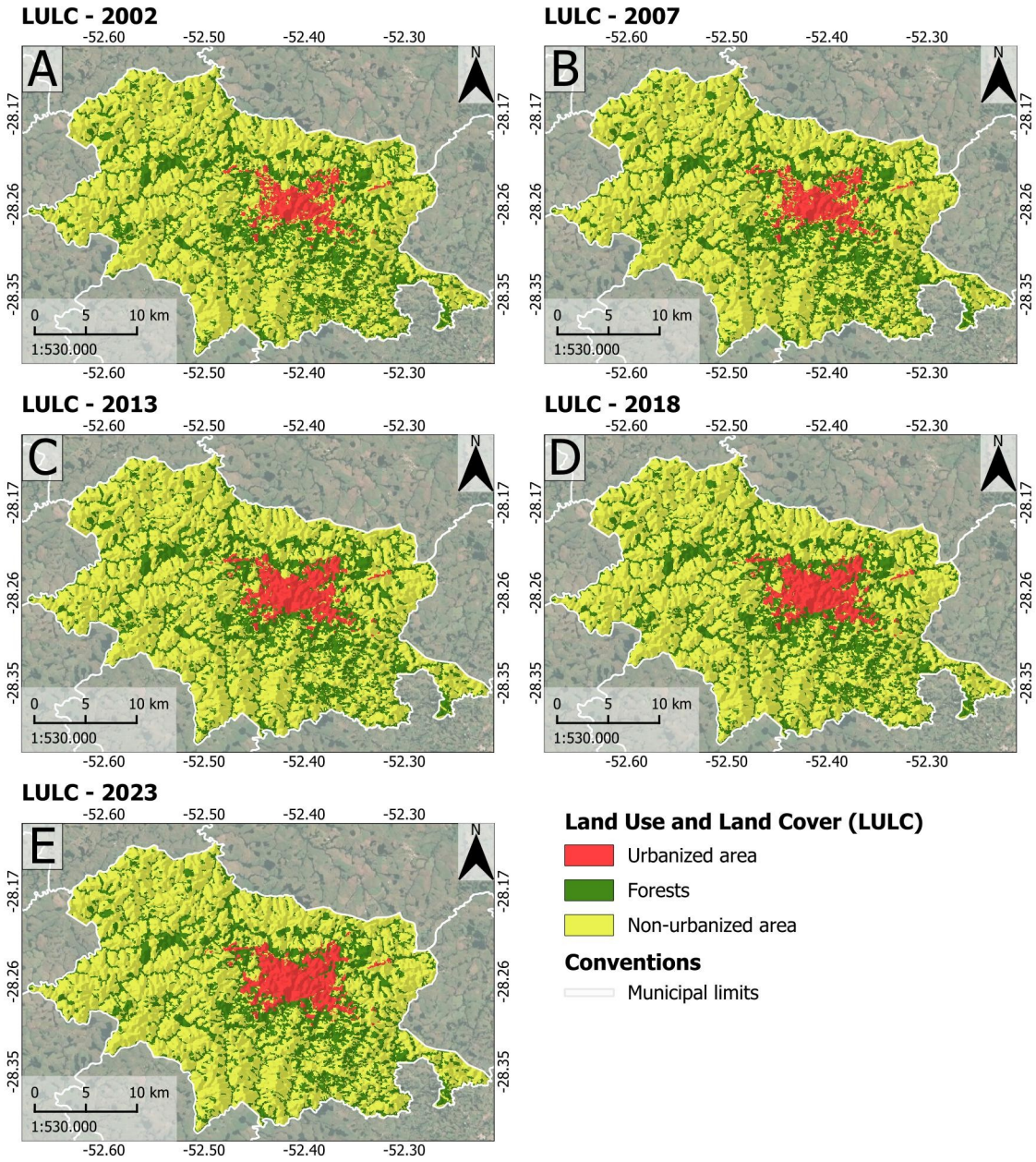

Figure 2. LULC maps produced through supervised classification of satellite images for the years 2002 (**A**), 2007 (**B**), 2013 (**C**), 2018 (**D**), and 2023 (**E**).

Table 2. Summary of the percentage of change in LULC in 2002, 2007, 2013, 2018 and 2023 in relation to the total area of the municipality of Passo Fundo.

LULC Classes	2002/2007 Δ%	2007/2013 Δ%	2013/2018 Δ%	2018/2023 Δ%	2002/2013 Δ%	2013/2023 Δ%	2002/2023 Δ%
Urbanized area	0.24%	1.10%	0.31%	0.30%	1.34%	0.61%	1.95%
Forests	−0.81%	−0.074%	−0.63%	−1.79%	−0.88%	−1.87%	−2.75%
Non-urbanized area	0.57%	−1.03%	−0.25%	1.49%	−0.46%	1.26%	0.80%

Table 2 demonstrates that forest areas gradually give way to urbanized and non-urbanized zones, revealing a continuous suppression and possible fragmentation of their patches over the analyzed time period ($\Delta\% = -2.75\%$, over approximately 20 years). These urbanized areas reveal themselves as a suppressive element in the surrounding areas, with consistently positive growth rates and an area (km^2) that increases continuously over time

($\Delta\% = 1.95\%$ over approximately 20 years). Meanwhile, non-urbanized areas reveal a more complex pattern of change, supporting an assertive interpretation, as they show less linear characteristics across all analyzed scenarios, with a tendency for their area to increase over a more extended period ($\Delta\% = 0.80\%$, over approximately 20 years).

It is worth noting that the most unusual scenario observed in Table 2 was the period between 2007 and 2013 (≈5 years), which showed a growth in the urbanized area close to half that of the expansion over the 20 years analyzed. It was noted that, in the most recent period, from 2018 to 2023, the greatest loss of forest area within the city occurred ($\Delta\% = -1.79\%$) over a 5-year period. This loss of forest areas occurred to a lesser extent through suppression by urbanized areas ($\Delta\% = 0.30\%$) and mainly due to the transition to non-urbanized areas ($\Delta\% = 1.49\%$), which was probably driven by agriculture and/or livestock farming, given the dominant activities for this LULC class. Agricultural and livestock activities change significantly with the season, varying in intensity and altering the optical properties of pixels and the visual representation on maps [64, 65].

In this Figure 3, urban evolution is represented by the urbanized areas mapped for the years 2002 (black), 2007 (dark gray), 2013 (purple), 2018 (light gray), and 2023 (white), highlighting the progressive expansion and consolidation of the urban fabric over the analyzed period. The spatial pattern indicates a continuous outward growth from the central urban core, with successive incorporation of surrounding areas over time. Forested areas (green scale) correspond to regions with denser arboreal vegetation cover, predominantly distributed in the peripheral portions of the study area, while non-urbanized areas (yellow scale) include agricultural lands, grasslands, pastures, and exposed soils. The interaction between urban expansion and surrounding land-use and land-cover classes reveals a gradual conversion of non-urbanized areas, particularly in zones adjacent to the urban perimeter, emphasizing the dynamics of land-use change associated with urban growth between 2002 and 2023. Through the urban expansion evolution map (Figure 3), it is possible to spatially visualize these transformations in the urbanized area class for 2002, 2007, 2013, 2018, and 2023, demonstrating an evolution, especially in 2013. The urbanized area patches closest to the urban center are increasingly consistent with each other, as shown in Figure 3, relative to the generated land use and land cover maps. These observed trends indicate a possible urban direction, capable of occupying urban voids, as reported by Cáceres et al. [66] and Moravej et al. [67], who state that this occurs in more consolidated, densely populated areas of the city.

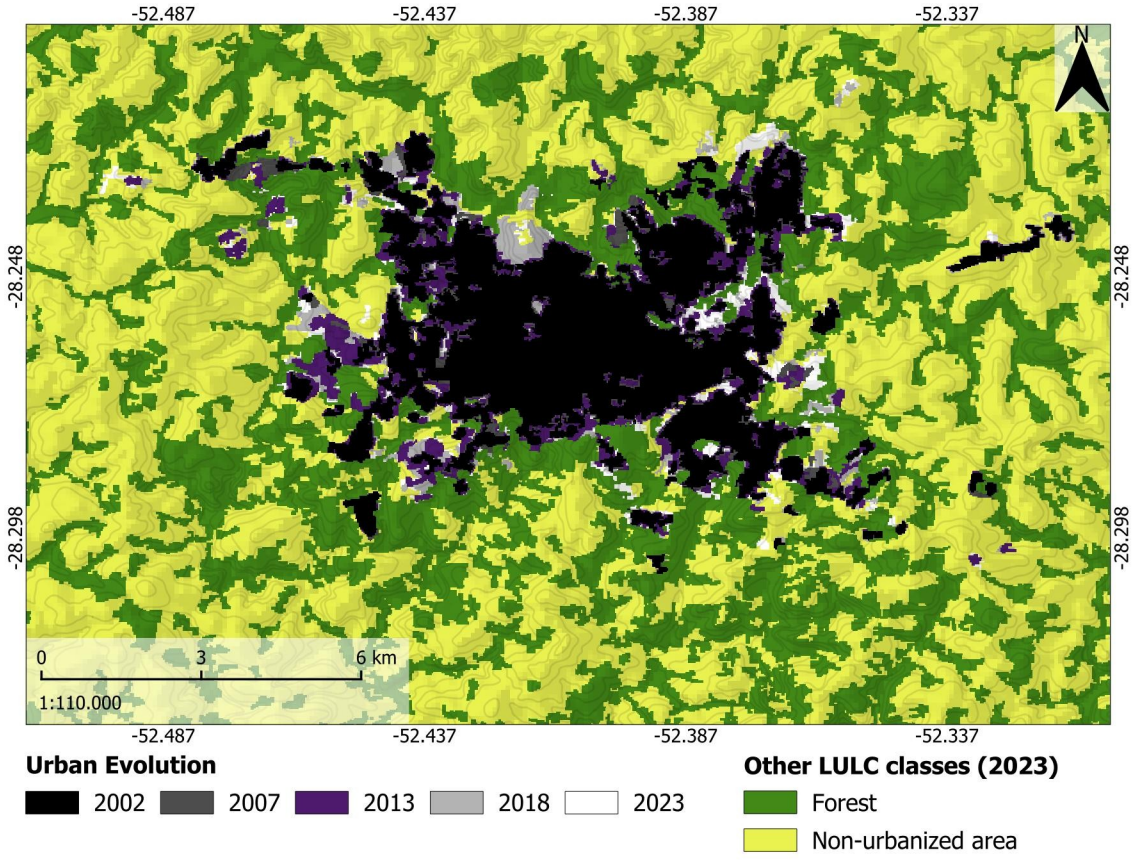

Figure 3. Map of the urban evolution in Passo Fundo for the years 2002, 2007, 2013, 2018, and 2023.

Table 3 shows the dimensions of changes in urbanized areas, analyzing this variable in isolation from the other LULC classes. For comparative analysis, official IBGE [29] data were presented, showing the city's population and growth during the analyzed periods. Analyzing these data (Table 3) and the map of urban expansion evolution (Figure 3), it is observed that, as urbanized areas continue to expand, the number of inhabitants has been increasing over time. In this context, it was observed that both the percentage of population growth and the percentage increase in the urbanized area in the period from 2002 to 2013 were greater than in the last 10 years. Specifically, the urbanized area shows growth approximately 3 times greater (31.41%) than in the most recent 10 years (10.87%). Over 20 years, the urbanized area increased by 45.71% and population growth was 23.24%, indicating that the city of Passo Fundo has expanded considerably, as shown in LULC data.

The mapping and quantification of LULC in the city of Passo Fundo proved adequate for understanding and representing urban expansion. However, a limitation of the methodological application is observed: population growth and urban expansion were not entirely proportional (for example, during the period from 2007 to 2013), leaving the causes of this finding unclear. This demonstrates that LULC provides a macro-scale view of the city's horizontal expansion and is relevant to the analysis of urban expansion indicators. To capture other dimensions of analysis, it was necessary to incorporate variables related to the dynamics of the city's vertical growth, enabling an integrated quantification of both horizontal and vertical expansion [67]. The database derived from the urban expansion simulation could provide a more nuanced understanding of these findings, generating consolidated projections to support future decision-making, including the implementation of public policies related to urban expansion, and may also serve as a reference for other cities worldwide [63, 67].

3.2. Mapping of Resistance and Direction Factors

The results of mapping the variables of resistance and direction factors enabled a spatial understanding of the quantitative data of each element analyzed within the limits of Passo Fundo (Figure 4). The proximity maps were essential for the CA-ANN model to quantify the relationships between the resistance and direction factors and the landscape factors (LULC), accounting for their spatial relationships.

Using Digital Elevation Model (DEM) data from the United States Geological Survey (USGS), a hypsometric map (Figure 5) was created. This cartographic element illustrates the altimetric variation of the city area of Passo Fundo, located in the state of Rio Grande do Sul, Brazil [29]. Altitudes were categorized into a range from the lowest points at 475 m to the highest points exceeding 725 m. Using a color scale, it is possible to identify the distinct topographic configurations that characterize the region of analysis. When analyzing the cartography, some characteristics are noted, such as the association of hydrography with areas of topographic depressions, where water flows around regions of lower altitude relative to the immediate vicinity, revealing a strong correlation between these two elements in the studied locality. It can be observed that the city's urban perimeter lies in some of the highest-altitude areas within the study area, predominantly between 630 m and 725 m.

Based on Pearson's correlation (Table 4), the main characteristics observed are moderate positive correlations between the urban center and the railways (0.47243) and the main roads (0.37837), indicating a close relationship between these infrastructures. In addition, a strong positive correlation (0.77410) is shown between the urban center and the secondary roads, reflecting the dense road network of the overlapping regions. Hypsometry exhibits moderate negative correlations with distance to main roads (-0.47), the urban center (-0.30), and railways (-0.43), indicating lower elevations closer to these features. This reveals that these variables are correlated with the city of Passo Fundo's topographic elevations and can help understand variables containing resistance and direction factors, which are related to each other, as determined by Gui et al. [26] and Qi et al. [68].

Table 3. Changes in urban area and estimated population over periods of approximately 5, 10, and 20 years.

Periods	Urban Area Changes (km^2)	Percentage Increase	Estimated Population (Inhabitants)	Percentage Increase
2002 to 2007	33.30 km^2 to 35.16	5.59%	174,107 to ≈185,882	≈6.76%
2007 to 2013	35.16 km^2 to 43.76	24.46%	≈185,882 to 194,432	4.60%
2013 to 2018	43.76 km^2 to 46.20	5.58%	194,432 to 201,767	3.77%
2018 to 2023	46.20 km^2 to 48.52	5.02%	201,767 to ≈214,564	≈6.34%
2002 to 2013	33.30 km^2 to 43.76	31.41%	174,107 to 194,432	11.67%
2013 to 2023	43.76 km^2 to 48.52	10.87%	194,432 to ≈214,564	≈10.35%
2002 to 2023	33.30 km^2 to 48.52	45.71%	174,107 to ≈214,564	≈23.24%

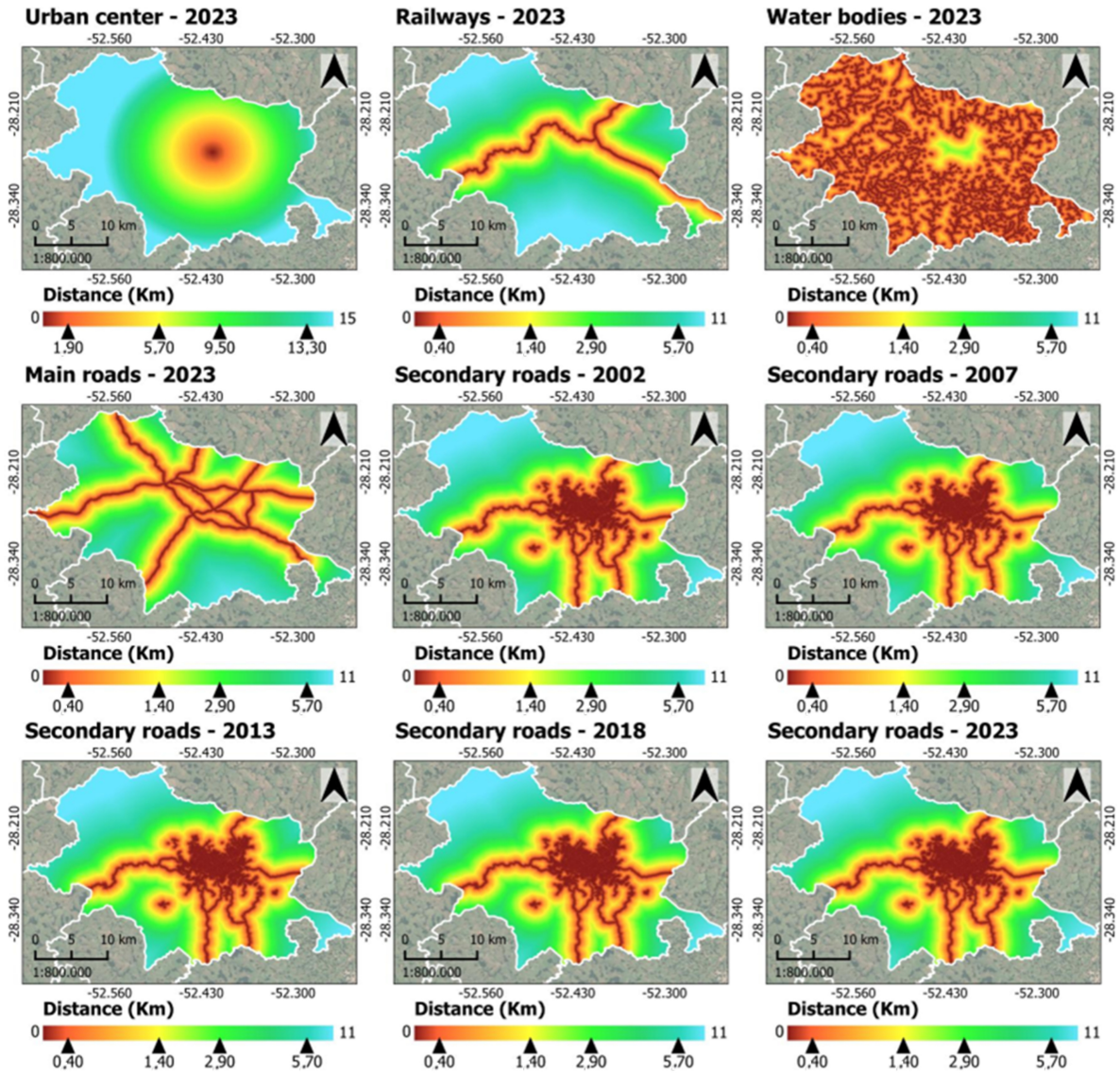

Figure 4. Proximity maps of the variables within the clusters of resistance factors and driving factors in the city of Passo Fundo.

3.3. Calibration of the CA-ANN Model

Calibration of parameters for the CA-ANN instrument. As a first step, the ANN parameters were defined to achieve the most suitable results for interpreting changes in LULC and, consequently, more reliable simulations [16, 20]. After several attempts to calibrate the parameters, it was concluded that the configuration achieved during the ANN training stage, as shown in Table 5, would yield the highest Number of Samples and the maximum possible value for the Maximum iterations parameter. To this end, 30,000 samples and 1,000 iterations were defined, so that the ANN-MLP Min. The Validation Overall Error decreased (Table 5), with a moderate number of simulation iterations per round. According to the studies by Khalid et al. [20] and Jain [25] the efficiency achieved by the model in simulating the scenarios in the testing phase, the neighbourhood, learning rate, hidden layers and momentum parameters were defined, described by Table 5, where the final parameters that generated the best results were inserted into the CA-ANN model to simulate the LULC scenarios in the testing phase, and subsequently, for the prediction of future LULC scenarios.

At the end of the ANN calibration, the CA configuration was defined, where it was observed that the best results were obtained with the LULC inputs (initial and final) with the longest time intervals (10 and 20 years) and with the fewest simulation iterations (1), prioritizing these parameters for the final simulations. The greater efficiency of these parameters occurs because, when considering longer time intervals, it results in a larger sample of changes in LULC, as well as, within the logic of CA operation, the fewest simulation iterations result in more reliable scenarios, considering a time frame more consistent in the relationship between the data input and the simulated period [20, 24, 25].

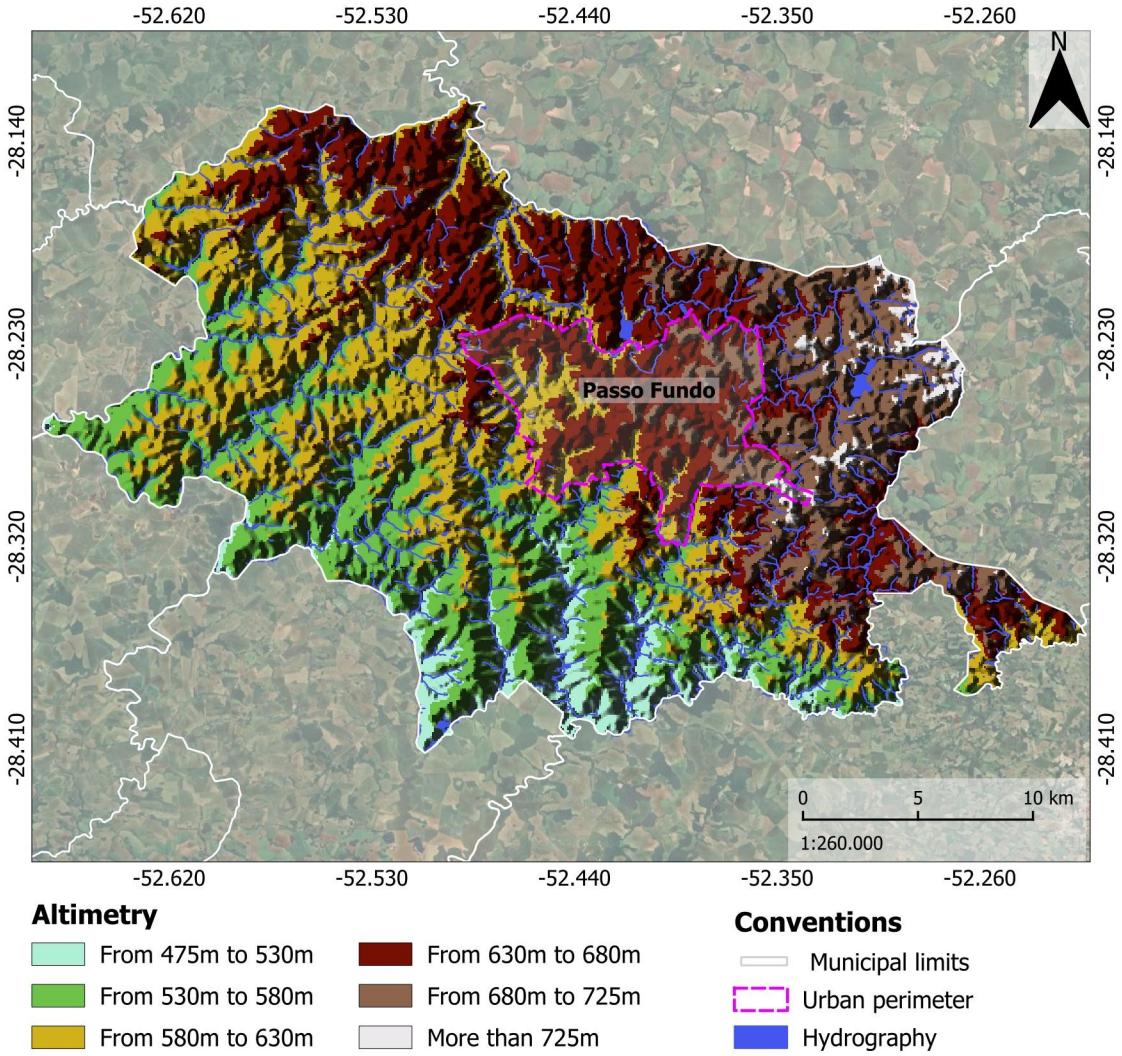

Figure 5. Map of the hypsometry variable in the city of Passo Fundo.

Table 4. Results of the Pearson Correlation between the variables of resistance and driving factors used in CA-ANN.

Variables	Hypsometry	Main Roads	Water Bodies	Urban Center	Railways	Secondary Roads
Hypsometry	–	−0.47031	0.20563	−0.30014	−0.43473	−0.02966
Main roads	–	–	−0.20013	0.37837	0.50504	0.18546
Water bodies	–	–	–	−0.22370	−0.14223	−0.09348
Urban center	–	–	–	–	0.47243	0.77410
Railways	–	–	–	–	–	0.54297
Secondary roads	–	–	–	–	–	–

Table 5. Final calibration parameters of the artificial neural network (ANN-MLP).

Parameters	Values
Number of Samples	30000
Neighbourhood	1
Learning rate	0.001
Maximum iterations	1000
Hidden Layers	10
Momentum	0.050

3.4. Testing Phase of the CA-ANN Model

Figure 6 presents the observed and simulated Land Use and Land Cover (LULC) maps for the years 2013, 2018, and 2023. Urbanized areas (red scale) are predominantly concentrated in the central portion of Passo Fundo, forming a consolidated urban core that progressively expands over time. From 2013 to 2023, both observed maps in Figure 6 demonstrate a growth pattern oriented toward the urban fringe, mainly over adjacent non-urbanized areas, indicating a consistent spatial trend of urban expansion. In this context, forested areas (green scale) are primarily distributed in peripheral and environmentally constrained regions and remain relatively stable throughout the analyzed period, although localized fragmentation can be observed near the urban–rural interface. Non-urbanized areas (yellow scale), which include agricultural lands, pastures, and exposed soils, dominate the landscape and represent the main land-use class converted into urban areas over time.

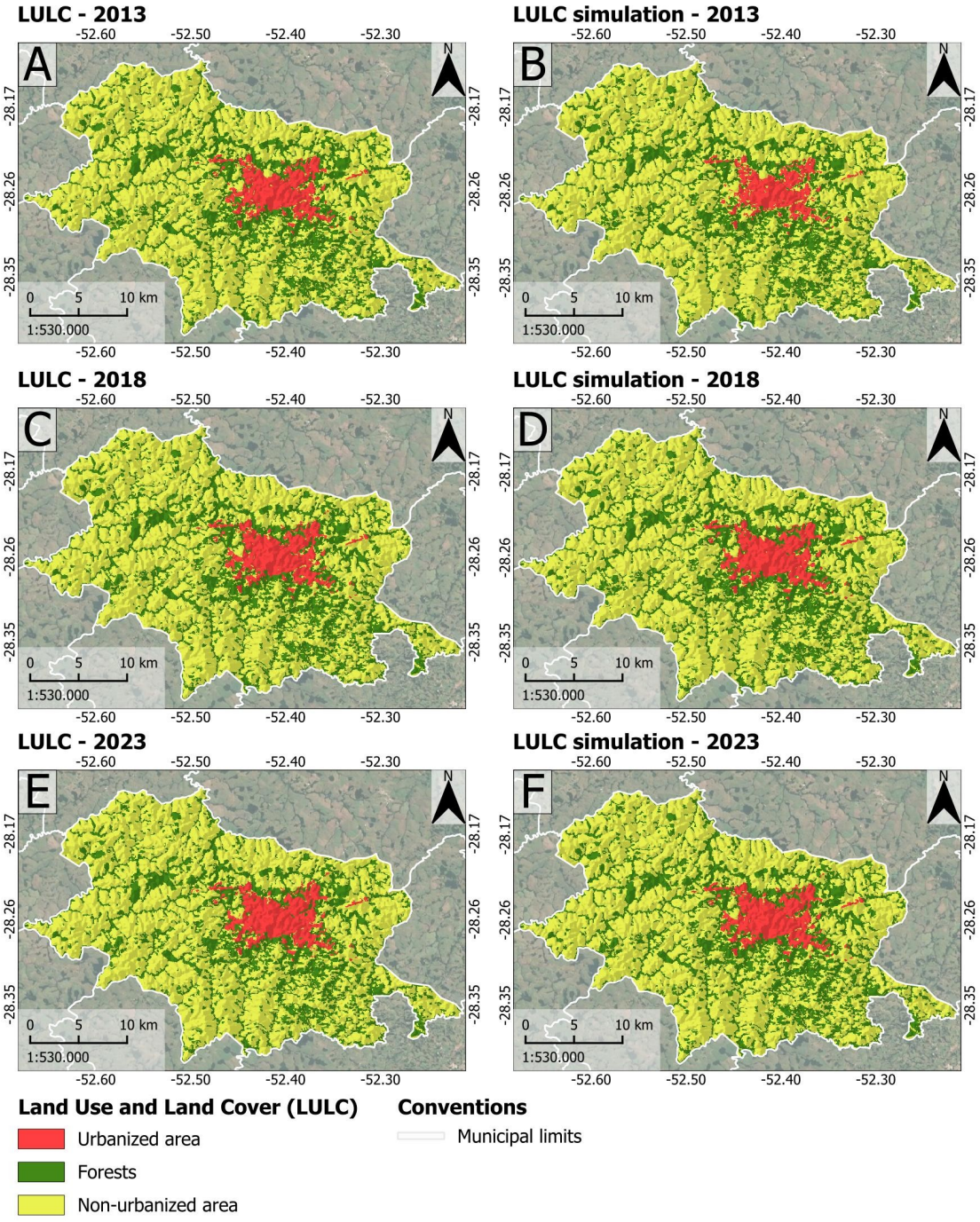

Figure 6. Results from the testing phase comparing LULC maps classified from satellite images for the years 2013 (**A**), 2018 (**C**), and 2023 (**E**), with the simulated LULC maps for 2013 (**B**), 2018 (**D**), and 2023 (**F**).

The main results of the simulations performed in the testing phase are shown in the mapping in Figure 6, which illustrates simulations from previous years (2013, 2018, and 2023), allowing the validation of the CA-ANN model based on consistent and verifiable data [24, 61]. To obtain these results, the ANN training parameters defined during model calibration (Table 5) were used, along with a simulation iteration count of 1 in the CA configuration. For the year 2013, the input LULC data from the years 2002 (initial) and 2007 (final) were used; for the 2018 simulation, the input LULC data from the years 2007 (initial) and 2013 (final) were used; For the year 2023, the input LULC data from the years 2013 (initial) and 2018 (final) were considered. The simulated maps (Figure 6) were compared to the LULC maps generated with supervised classification of satellite images (Figure 2), allowing the model's accuracy in replicating the observed conditions for the analyzed year to be evaluated.

In addition to the spatial data obtained through cartography, quantitative data were generated to comparatively describe (Table 6) the changes between LULC classified from satellite images, and LULC generated through simulations within predefined periods, allowing a quantitative analysis of the efficiency of the CA-ANN model for LULC simulation. These data, presented in Table 6, indicate that the 2013 simulation showed a large difference in LULC classes, with the urbanized area showing the highest proportional error among the analyzed categories. For the other classes, the error is less relevant given the city's overall area. The results of the ANN training validation showed a low minimum validation error (0.03208) and a high Kappa index (0.91288). The validation of the LULC map simulation indicated an accuracy of 95.59% and a Kappa index of 0.90910, demonstrating adequate precision for LULC simulation in the study area.

Despite the positive indicators, the focus on the urbanized area class revealed that the simulation for 2013 estimated an urbanized area of 37.15 km^2 (Table 6), a value significantly lower than that obtained from satellite imagery (43.76 km^2), representing a difference of approximately 15%. This discrepancy stems from the inconsistency in urban growth between 2007 and 2013, a period during which expansion occurred outside the pattern observed between 2002 and 2007. These patterns arise from external factors, as urban fringe areas are more susceptible to irregular residential invasions, given the lower urban land values at the city outskirts when compared to the real estate speculation values observed in the central area of Passo Fundo. The algorithm projected 2013 based on the repetition of the previous pattern, which prevented it from predicting the anomalous growth that occurred. These results, while imprecise, highlight a limitation of the methodology in the face of abrupt changes in the pattern of urban expansion, influenced by highly variable factors and difficult prediction [61].

Unlike the 2013 simulation, the results in Table 6 are satisfactory, with good model accuracy in simulating changes in LULC proportions. An error of only 0.86 km^2 more urbanized area, 0.55 km^2 more forested areas, and 1.41 km^2 less non-urbanized areas was observed, demonstrating good predictive capacity to represent urban expansion and its impact on the other classes, generating environmental consequences from forest loss, particularly with respect to biodiversity, ecosystem services, and urban planning. ANN training validation yielded a minimum validation error of 0.03124 and a Kappa index of 0.92314, confirming the model's consistent, accurate performance in simulating LULC changes. Validation of the simulated 2018 map against LULC derived from satellite imagery yielded 97.41% accuracy and a Kappa index of 0.94762, indicating adequate model performance. These results demonstrate a satisfactory ability to reproduce the characteristics of the 2018 LULC, with good agreement between the simulated data and satellite imagery.

Table 6. Areas and proportions of LULC classes derived from satellite images and simulated LULC data for the years 2013, 2018, and 2023.

Year	LULC Class	Classification (km^2)	Simulation (km^2)	Δ (km^2)	Δ (%)
2013	Urbanized area	43.76	37.15	6.61	−0.85
	Forests	233.47	230.73	2.74	−0.35
	Non-urbanized area	503.3	512.64	−9.35	1.2
2018	Urbanized area	46.24	47.1	0.86	0.11
	Forests	233.01	233.56	0.55	0.07
	Non-urbanized area	501.14	499.73	−1.41	−0.18
2023	Urbanized area	48.52	47.58	−0.93	−0.12
	Forests	218.93	232.75	13.81	1.77
	Non-urbanized area	512.85	499.97	−12.88	−1.65

As shown in Table 6, the simulation for 2023 indicated a difference of -12.88 km^2 for the non-urbanized area class and $+13.81$ km^2 for forested areas, compared to the LULC derived from satellite image classification. However, as observed in the 2018 simulation, the results were consistent across the urbanized area class, with an error of only 0.93 km^2 relative to the proportions derived from the images, which can be considered a satisfactory result given the analysis's main focus on this class. The ANN training-validation set showed the lowest minimum error among all simulations (0.01901) and a Kappa index of 0.90533, indicating high coherence in reproducing the data patterns. Validation of the simulated LULC map based on 2023 satellite imagery showed an accuracy of 97.55% and a Kappa index of 0.95008, demonstrating that the model overall accurately represented the characteristics of the urbanized area within the city of Passo Fundo.

Tests demonstrated the good efficiency of the CA-ANN model in simulating LULC within the limits of Passo Fundo. 2013 presented the largest proportional area error compared to the other simulations, with 15.11% less urbanized area than the reference LULC map, while the 2018 and 2023 simulations registered errors of 1.86% and -1.92%, respectively, for the urbanized area class, demonstrating satisfactory results for the last two simulations, with 2018 being the year with the most consistent predictions of changes in LULC classes.

The evaluative metrics applied to the maps may not fully reflect the model's efficiency in predicting urban expansion, as the MOLUSCE tool does not allow isolating LULC classes for individual validation of quantitative data and maps. In this sense, the analysis of LULC classes in isolation allowed us to observe differences proportional to the total area of each class, making it possible, according to Khalid et al. [20] and Jain [25], to identify the proportions with the changes detected in the environment with greater precision, demonstrating a high reliability of the analyzed time period.

3.5. Simulation of Future Scenarios with CA-ANN

The first simulation of a future urban expansion scenario using LULC was conducted to predict changes for 2033. To generate the LULC simulation for 2033, the 2013 initial and 2023 final LULC maps were used, with the CA simulation limited to 1 iteration. The cartographic results of the 2033 simulation are shown in Figure 7B, along with the 2023 land use and land cover map (Figure 7A), for graphical comparison of LULC class changes. The validation process for the artificial neural network (ANN-MLP) training yielded consistent results [56, 69]. The model achieved a low minimum validation error (0.02743) and a Kappa index of 0.93595. These data indicate that the ANN performs well in predicting the transition potential of LULC classes.

Based on the quantitative data presented in Table 7, it is possible to observe changes in land use and land cover proportions, indicating trends in the city's configuration in 2033. A notable increase of 3.66 km^2 in the urbanized area is observed, accompanied by a reduction of 3.30 km^2 in the forested area and a decrease of 0.36 km^2 in non-urbanized areas. These data suggest that, among all LULC classes, only the urbanized area expanded its territory. While the other courses experienced contraction, these quantitative variations reflect patterns of increasing urbanization, with a direct impact on green areas, suggesting a possible intensification of urban occupation in areas near the city limits in the future [70, 71].

The land use and land cover simulation mapping for the year 2043 is shown in Figure 7C, which can be compared with the LULC map from the most recent date when supervised classification was performed, in the year 2023 (Figure 7A). The simulation was performed using inputs from the years 2002 (initial) and 2023 (final). The 20-year interval was combined with a simulation iteration value of 1, so the algorithm could interpret patterns from the past 20 years and replicate them in a future scenario. Validation of the ANN training stage revealed good performance of the artificial neural network model (ANN-MLP) for predicting the transition potential of land use and land cover classes, with Kappa index values of 0.91843 and a minimum validation error of 0.03708. Based on the quantitative description of each LULC class, Table 7 shows that the urbanized area increased by 6.83 km^2 from 2023. This indicates that, in this scenario, the urbanization of the region suppressed a large part of the forests (2.98 km^2) and some areas previously classified as non-urbanized (3.85 km^2) over the 20 years observed in the CA-ANN simulation. Table 7 shows that, in 2033, the largest discrepancy occurs in the urbanized area, where the model overestimates the observed area by 3.66 km^2 (0.47%). In contrast, forest and non-urbanized classes present marginal underestimations, with differences below 0.5%, indicating a high level of agreement between the simulated values. Subsequently, in the 2043 scenario, forest and non-urbanized areas maintain moderate negative differences (-0.38% and -0.49%, respectively). These results suggest that the model tends to prioritize urban expansion, mainly reallocating non-urbanized areas and, to a lesser extent, forested areas as a consequence of urban growth.

This simulated expansion pattern highlights that urban growth is advancing predominantly in non-urbanized areas, which in this case are mainly agricultural and pasture lands. Such dynamics indicate a land-use conflict between urban development and agricultural functionality. The ongoing conversion of rural productive territories threatens the continuity of food systems, ecosystem services, and the livelihoods of rural populations. This conflict shows the broader territorial disputes frequently observed in medium-sized cities across the Global South, where limited governance instruments often fail to prevent spatial competition between urban and agricultural interests.

The differences in LULC between the 2043 forecast and the 2033 simulation indicate the trend of future urban expansion in Passo Fundo over this 10-year interval. This phenomenon can be seen in the 3.17 km^2 increase in urbanized areas, which occurred at the expense of neighboring land uses. The results of quantifying forest areas

(0.32 km^2), while positive, represent only 0.04% of the city area, indicating that for this period (2033 to 2043), the trend is that this variable will not be significantly altered. To provide a unified understanding of the LULC simulations for 2033 and 2043, a map was created showing the evolution of urbanized area classes across the study area, starting in 2023. This graphic data (Figure 8) can be analyzed in conjunction with Table 8, which provides quantitative data on changes in urbanized areas within the scope of the simulated scenarios, providing a better understanding of LULC changes over the 20 future years simulated with the CA-ANN instrument.

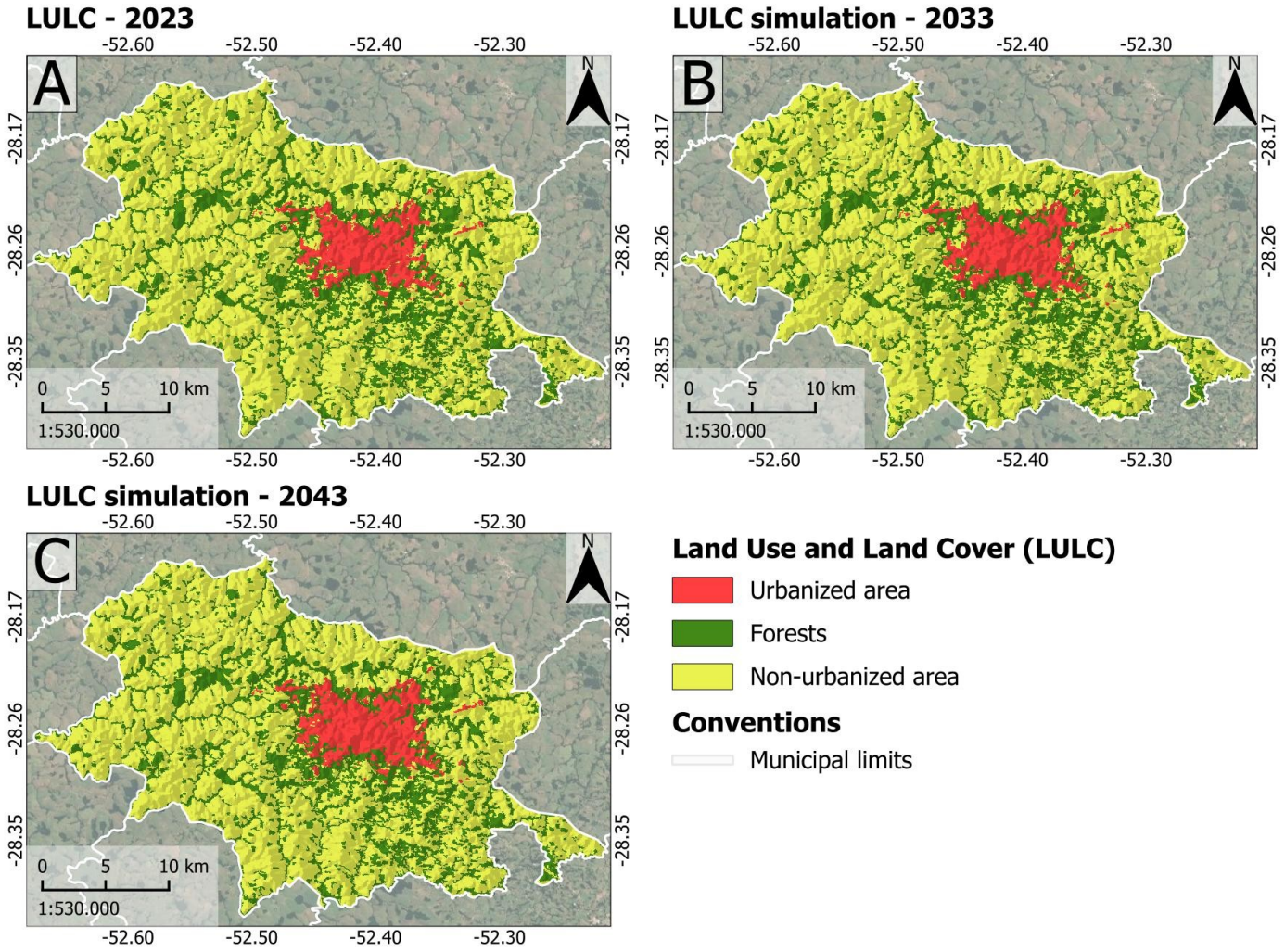

Figure 7. Mapping of the supervised LULC classification data for 2023 (**A**) and the maps showing the results of the LULC simulations for 2033 (**B**) and 2043 (**C**).

Table 7. Areas and proportions of LULC classes derived from satellite images and simulated LULC data for the years 2033 and 2043.

Year	LULC Class	Classification (km^2)	Simulation (km^2)	Δ (km^2)	Δ (%)
2033	Urbanized area	48.52	52.18	3.66	0.47
	Forests	218.93	215.64	−3.30	−0.42
	Non-urbanized area	513.24	512.88	−0.36	−0.046
2043	Urbanized area	48.52	55.35	6.83	0.87
	Forests	218.93	215.95	−2.98	−0.38
	Non-urbanized area	513.24	509.39	−3.85	−0.49

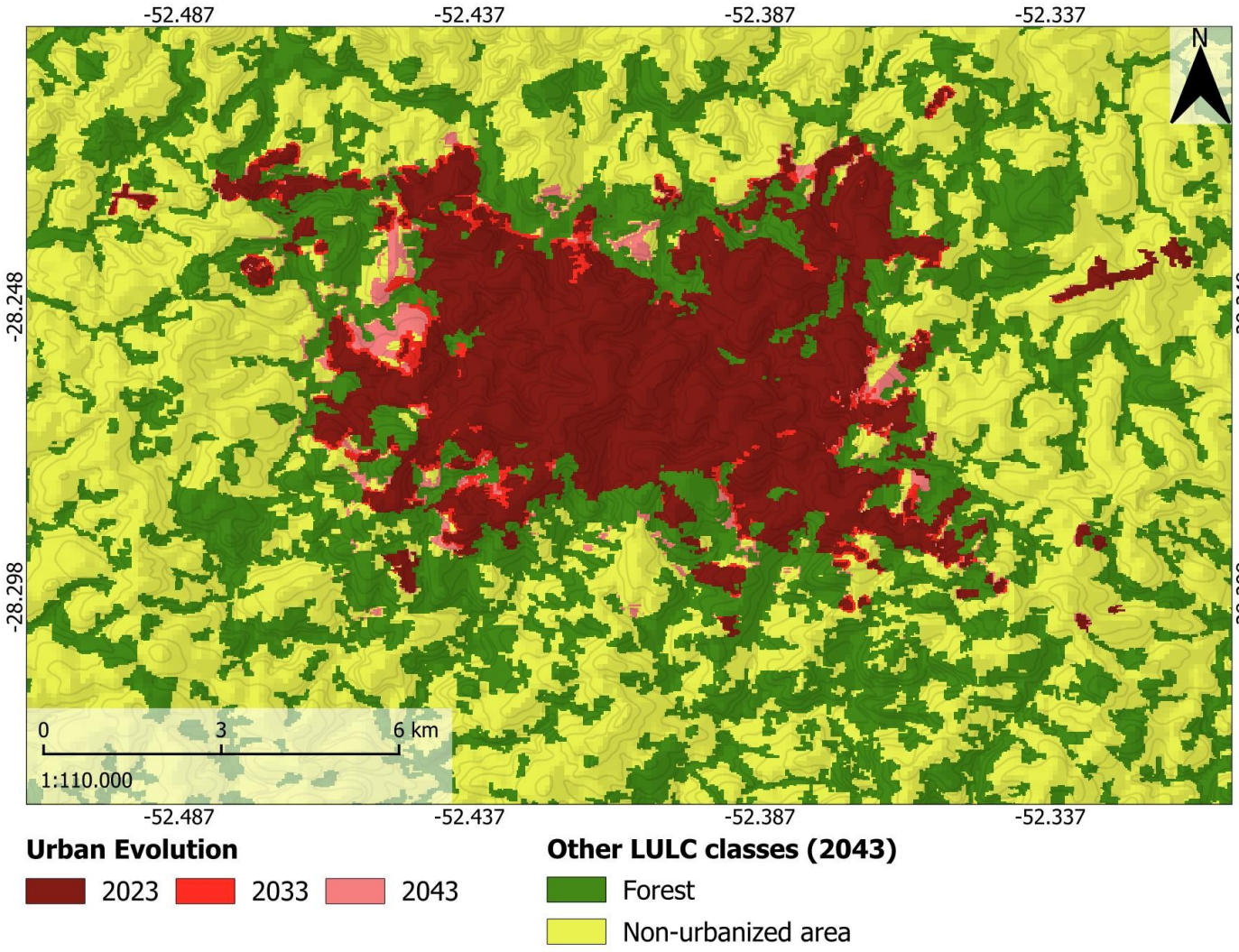

Figure 8. Map of urban evolution in the city of Passo Fundo, starting from the year 2023, showing simulated data for the years 2033 and 2043.

Table 8. Summary of changes in the urban area class during the simulated periods, considering the individual area of the variable itself.

Periods	Urban Area Changes	Urban Area Increase (%)
2033 to 2043	52.18 km^2 to 55.35 km^2	6.08
2023 to 2033	48.52 km^2 to 52.18 km^2	7.54
2023 to 2043	48.52 km^2 to 55.35 km^2	14.08
2002 to 2033	33.30 km^2 to 52.18 km^2	56.70
2002 to 2043	33.30 km^2 to 55.35 km^2	66.21

Based on an analysis of the data in Table 8 and Figure 8, it is understood that the urban expansion of Passo Fundo, based on observations from the 2033 and 2043 simulations, follows a moderately increasing urbanization rate, considering that the simulated years indicate an increase in urbanized areas throughout the analyzed periods since 2002. From the initial year of 2002 to 2043, the city of Passo Fundo is predicted to experience a 66.21% increase in its total urbanized area. The simulations indicate a 14.08% increase in the urbanized area between 2023 and 2043. Based on the analysis, this growth will occur in a dispersed manner, mainly in the western region, followed by less expansion to the north and east relative to the current urban perimeter. It is noteworthy that the forest class, despite offering some resistance to the urbanized area class, is constantly being suppressed by the other

LULC classes (especially in recent years), having an initial area of 240.48 km^2 in 2002, with a projected reduction to 215.95 km^2 by the year 2043 (-10.20%).

As noted in the results description, the MOLUSCE tool yielded primarily satisfactory data. However, some reservations were noted regarding certain plugin functionalities, which were discussed throughout the text. The central reservation is the lack of a function to validate land use and land cover classes individually, making it impossible to evaluate the model's efficiency in predicting each LULC class. It was only possible to analyze it in conjunction with the other classes at the territorial scale, where the urbanized area represents approximately 7% of the total area in 2043, rendering the validation analysis disproportionate.

Tola and Deyassa [61] presented their objects of study at scales similar to the city of Passo Fundo. The study by Baidoo et al. [72] observed that the city studied showed a similar rate of expansion, despite its larger scale. In this context, the results of the urban expansion simulation of the city of Passo Fundo showed some agreement with the expansion of cities of different scales and locations worldwide, suggesting that the projections follow a path aligned with what may occur in reality.

4. Conclusions

The simulations demonstrated satisfactory results for understanding current scenarios based on the collected data on land use and land cover within the city's boundaries. The analyses revealed moderate-scale growth of the city during the analyzed period, totaling a 45.71% increase in urbanized area from 2002 to 2023, with simulations indicating an additional increase of at least 14.08% by 2043. This growth in urban areas indicated a 10.20% decrease in forest areas from 2002 to 2043. In this context, it was concluded that although the CA-ANN instrument with the MOLUSCE plugin presented certain limitations in its execution, the results showed good indicators of the proportions and directions of the expansion of the city of Passo Fundo, and can be used in new urban projects, relating to the future impacts of urban expansion.

It has been observed that Passo Fundo is expanding, underscoring the need to plan for its growth. The projected 66.21% expansion of the urbanized area from 2002 to 2043 reveals that the impact of this urbanization is heading towards a future that requires planning. The public body responsible for managing the city has a duty to design the urban environment, aiming for sustainable development, based on in-depth studies of the urban area. This allows for more efficient resource management in implementing public infrastructure in areas of the city experiencing the greatest growth, thereby enabling the control or mitigation of environmental degradation caused by urban expansion, as observed in the predictive results.

Based on the findings throughout the study, and considering the results obtained and the entire process carried out with the CA-ANN instrument used in the MOLUSCE plugin, some improvements were defined that could be made within the tool itself. Since QGIS is open-source software, there are plugins like MOLUSCE created by users. In this context, the suggested improvements are: (1) A tool within the plugin itself to perform the alignment of input rasters for the ANN: considering that MOLUSCE prevents the creation of simulations if the input layers are not proportionally aligned, the availability of a tool that makes this process easier is a good option. (2) A way to automatically export tables and graphs directly to spreadsheet software, considering that this process has become excessively time-consuming due to the various tests and applications, this suggestion would have the positive consequence of saving time in exporting the generated data.

A validation method for each of the LULC classes. This is the functionality most relevant to obtaining more reliable validation results (3). (4) The option to add as many LULC maps as necessary to the input layer, because in this way, the ANN can be calibrated to interpret all LULCs at the same time, enabling the model to predict scenarios based on the patterns found in various LULC maps, increasing the amount of data analyzed simultaneously. (5) A tab with a user manual for the tool: providing more specific details from the methodological application to the description of the algorithms and formulas that make up the model.

These considerations can be applied to the creation of proprietary software for LULC simulation. Creating a system independent of the QGIS environment would provide greater flexibility, enabling the implementation of more advanced and customized functionality and ensuring greater control over the program's code and structure. By avoiding dependence on plugins that are frequently incompatible with new versions of QGIS, it would be possible to ensure a more stable, long-term tool better adapted to the specific needs of LULC studies.

These findings reinforce the need for integrative land use policies capable of balancing urban development with the preservation of agricultural and ecologically significant areas. By identifying areas at risk of land-use conflict, simulation models such as CA-ANN can support evidence-based decision-making and proactive spatial planning. In this context, sustainable land governance becomes a strategic way—particularly in mid-sized cities of the Global South—where urban expansion increasingly overlaps with agribusiness zones, compromising food security, biodiversity, and long-term rural productivity.

Author Contributions

G.P.S.: Conceptualization, Investigation, Supervision; E.G.: Validation, Writing—original draft; B.W.B.: Investigation, Validation: M.R.d.S.: Visualization, Validation; Writing—review & editing; G.M.: Investigation, Validatation; G.T.C.: Data curation, Formal analysis; Validation; R.T.L.: Data curation, Formal analysis, Validation; A.N.: Data curation, Formal analysis, Writing—original draft. All authors have read and agreed to the published version of the manuscript.

Funding

National Natural Science Foundation of China [grant number W2431031].

Institutional Review Board Statement

Not applicable.

Informed Consent Statement

Not applicable.

Data Availability Statement

Data used in this paper are available from author upon request.

Acknowledgments

The authors acknowledge the United States Geological Survey (USGS) for providing the images from the Landsat 7 and Landsat 8 satellites. The authors acknowledge the European Space Agency (ESA) for providing the unpublished and processed images from the Sentinel-5P satellite. We are grateful to the Center for Studies and Research on Urban Mobility (NEPMOUR+S/ATITUS); the Market, Innovation and Sustainability Research Group (Atitus); the Foundation for Research and Innovation of the State of Santa Catarina (Fapesc), Santa Catarina, Brazil; the Meridional Foundation, Brazil; the National Council for Scientific and Technological Development (CNPq), Brazil; and the Atlantic International Research Center (AIR Center) for granting a doctoral scholarship through the Foundation for Science and Technology in Portugal, and IB-S (Institute of Science and Innovation for Bio-Sustainability) UMinho. This work was supported by FCT—Fundação para a Ciência e Tecnologia, IP, by project reference: PRT/BD/154704/2023, and identifier DOI: https://doi.org/10.54499/PRT/BD/154704/2023.

Conflicts of Interest

The authors declare that they have no known competing financial interests or personal relationships that could have appeared to influence the work reported in this paper. Co-author Alcindo Neckel is an Editorial Board Member of this journal was not involved in the review processing or decision to accept this paper.

Use of AI and AI-Assisted Technologies

No AI tools were utilized for this paper.

References

1. Chen, L.; Gong, C.; Guo, Y.; et al. Integrating macro-micro perspectives to measure urban land expansion in Minsk, Belarus. *J. Urban Manag.* **2025**, *14*, 1–13. https://doi.org/10.1016/j.jum.2025.06.012
2. Wang, H.; Wang, Q.; Zhang, X.; et al. Mapping global annual urban land cover fractions (2001–2020) derived with multi-objective deep learning. *Int. J. Appl. Earth Obs. Geoinf.* **2025**, *136*, 104404. https://doi.org/10.1016/j.jag.2025.104404
3. González-Calle, J.L. Metropolitan expansion and rural change in the peri-urban edge Medellín—Rionegro (Colombia). *J. Urban Manag.* **2024**, *13*, 521–540. https://doi.org/10.1016/j.jum.2024.05.007
4. Liu, S.; Wang, Y.; Gong, P.; et al. Regional warming from urbanization is disproportionate to urban expansion rate. *One Earth* **2025**, *8*, 101234. https://doi.org/10.1016/j.oneear.2025.101234
5. Kafy, A.A.; Dey, N.N.; Saha, M.; et al. Leveraging machine learning algorithms in dynamic modeling of urban expansion, surface heat islands, and carbon storage for sustainable environmental management in coastal ecosystems. *J. Environ. Manag.* **2024**, *370*, 122427. https://doi.org/10.1016/j.jenvman.2024.122427
6. Almulhim, A.I.; Cobbinah, P.B. Dammam metropolitan area: Advancing the pursuit of urban resilience. *Habitat Int.* **2025**, *163*, 103499. https://doi.org/10.1016/j.habitatint.2025.103499
7. Neckel, A.; Da Silva, J.L.; Saraiva, P.P.; et al. Estimation of the economic value of urban parks in Brazil, the case of the City of Passo Fundo. *J. Clean. Prod.* **2020**, *264*, 121369. https://doi.org/10.1016/j.jclepro.2020.121369
8. Mânica, A.N.; Rocha, C.; Araújo, L.S.; et al. From forest to urban: Assessing the impact of land cover on water quality. *J. Environ. Manag.* **2025**, *386*, 125739. https://doi.org/10.1016/j.jenvman.2025.125739
9. Dehghani, A.; Soltani, A.; Nateghi, K. Balancing urban growth and Environmental change: Land use patterns in Tehran and Sydney. *Environ. Sustain. Indic.* **2025**, *26*, 100691. https://doi.org/10.1016/j.indic.2025.100691
10. Ogara, D.A.; Akrofi, M.M.; Muthoni, V. Understanding the socio-economic and environmental effects of Port Development on urban and marine environments: A case of Mombasa Port expansion (2006–2021) on urban and marine environments in Kenya. *Ocean Coast. Manag.* **2025**, *267*, 107581. https://doi.org/10.1016/j.ocecoaman.2025.107581
11. Silva, L.F.; Lozano, L.P.; Oliveira, M.L.; et al. Identification of hazardous nanoparticles present in the Caribbean Sea for the allocation of future preservation projects. *Mar. Pollut. Bull.* **2021**, *168*, 112425. https://doi.org/10.1016/j.marpolbul.2021.112425
12. Soares, F.; Silva, M.; Azevedo, I. Urban decarbonization policies and strategies: A sectoral review. *Renew. Sustain. Energy Rev.* **2025**, *215*, 115617. https://doi.org/10.1016/j.rser.2025.115617
13. Liu, C.; Yuan, X.; Ni, G.; et al. Utilizing deep transfer learning to discover changes in landscape patterns in urban wetland parks based on multispectral remote sensing. *Ecol. Inform.* **2024**, *83*, 102808. https://doi.org/10.1016/j.ecoinf.2024.102808
14. De, S.; Das, A.; Mazumder, T.N. A systematic literature review of remote sensing approaches in urban green space research: Towards achieving sustainable development goals. *Urban Clim.* **2025**, *59*, 102332. https://doi.org/10.1016/j.uclim.2025.102332
15. Nkonu, R.S.; Antwi, M. A novel ANN-CA and MCDA integrated framework for predicting urban expansion and its implications on future flood risk, Accra Metropolis. *Environ. Dev.* **2024**, *52*, 101061. https://doi.org/10.1016/j.envdev.2024.101061
16. Amoah, M.K.M.; Gorsevski, P.V. Predicting land use land cover changes and impact on urban wetlands using cellular automata and artificial neural networks approach, a case study in Greater Accra, Ghana. *Sci. Afr.* **2025**, *28*, e02767. https://doi.org/10.1016/j.sciaf.2025.e02767
17. Onsay, E.A.; Carilo, S.A.; Baltar, K.C. Measuring vote-selling and modeling electoral behavior of students and professionals in the Philippine election: Evidence from econometric modeling, machine learning, and Artificial Neural Networks (ANN). *DSEF* **2025**, *7*, 100062. https://doi.org/10.1016/j.dsef.2025.100062
18. Shukla, A.; Pachauri, R.K.; Hussain, A.; et al. Comparative analysis dust accumulation impact on PV performance using artificial neural network and machine learning algorithms. *Results Eng.* **2025**, *26*, 105024. https://doi.org/10.1016/j.rineng.2025.105024

19. Adhab, A.H.; Mahdi, M.S.; Shukla, M.; et al. Estimation of activity coefficient of aqueous ionic liquids using a machine learning method: The artificial neural network coupled with group contribution approach. *J. Indian Chem. Soc.* **2025**, *102*, 101924. http://dx.doi.org/10.1016/j.jics.2025.101924
20. Khalid, W.; Shamim, S.K.; Ahmad, A. Synergistic approach for land use and land cover dynamics prediction in Uttarakhand using cellular automata and artificial neural network. *Geomatica*, **2024**, *76*, 100017. https://doi.org/10.1016/j.geomat.2024.100017
21. Li, S.; Lin, W. A hybrid landscape metric-enhanced cellular automata model (LE-CA) for land use/land cover change simulation: An application to coastal wetlands. *Ecol. Model.* **2025**, *508*, 111209. https://doi.org/10.1016/j.ecolmodel.2025.111209
22. Panda, K.C.; Singh, R.M.; Singh, S.K. Advanced CMD predictor screening approach coupled with cellular automata-artificial neural network algorithm for efficient land use-land cover change prediction. *J. Clean. Prod.* **2024**, *449*, 141822. https://doi.org/10.1016/j.jclepro.2024.141822
23. Mansour, S.; Alotaibi, O.; Alnasrallah, M. Geospatial modelling of urban expansion effects on the land ecosystems in Kuwait using random forest and cellular automata. *J. Urban Manag.* **2025**, *22*, 44–58. https://doi.org/10.1016/j.jum.2025.05.011
24. Roy, S.K.; Alam, M.T.; Mojumder, P.; et al. Dynamic assessment and prediction of land use alterations influence on ecosystem service value: A pathway to environmental sustainability. *Environ. Sustain. Indic.* **2024**, *21*, 100319. https://doi.org/10.1016/j.indic.2023.100319
25. Jain, M. Future land use and land cover simulations with cellular automata-based artificial neural network: A case study over Delhi megacity (India). *Heliyon* **2024**, *10*, e34662. https://doi.org/10.1016/j.heliyon.2024.e34662
26. Gui, B.; Bhardwaj, A.; Sam, L. Cellular automata models for simulation and prediction of urban land use change: Development and prospects. *Artif. Intell. Geosci.* **2025**, *6*, 100142. https://doi.org/10.1016/j.aiig.2025.100142
27. Zhou, Z.; Chen, Y.; Wang, Z.; et al. Integrating cellular automata with long short-term memory neural network to simulate urban expansion using time-series data. *Int. J. Appl. Earth Obs. Geoinf.* **2024**, *127*, 103676. https://doi.org/10.1016/j.jag.2024.103676
28. Gharaibeh, A.A.; Al-Rabee, M.S.; Obeidat, R. Integrating artificial neural networks and neighborhood analysis for enhanced urban growth prediction depending on planned future development areas: A case study of Ar-Ramtha, Jordan. *J. Urban Manag.* **2025**, *14*, 1179–1201. https://doi.org/10.1016/j.jum.2025.04.010
29. IBGE (Brazilian Institute of Geography and Statistics). Cities and States: Passo Fundo, Brazil, 2025. Official Website: https://cidades.ibge.gov.br/brasil/rs/passo-fundo/panorama
30. Bodah, B.W.; Neckel, A.; Maculan, L.S.; et al. Sentinel-5P TROPOMI satellite application for NO_2 and CO studies aiming at environmental valuation. *J. Clean. Prod.* **2022**, *357*, 131960. https://doi.org/10.1016/j.jclepro.2022.131960
31. Llavero-Pasquina, M. Driving ecologically unequal exchange: A global analysis of multinational corporations' role in environmental conflicts. *Glob. Environ. Change* **2025**, *92*, 103006. https://doi.org/10.1016/j.gloenvcha.2025.103006
32. Neckel, A.; Goellner, E.; Oliveira, M.L.; et al. Geospatial applicability optics of the TROPOspheric monitoring instrument (TROPOMI) on a global scale: An overview. *Geosci. Front.* **2025**, *16*, 102008. https://doi.org/10.1016/j.gsf.2025.102008
33. Pan, X.; Liu, Z.; He, C.; et al. Modeling urban expansion by integrating a convolutional neural network and a recurrent neural network. *Int. J. Appl. Earth Obs. Geoinf.* **2022**, 112, 102977. https://doi.org/10.1016/j.jag.2022.102977
34. Rifat, S.A.A.; Liu, W. Predicting future urban growth scenarios and potential urban flood exposure using Artificial Neural Network-Markov Chain model in Miami Metropolitan Area. *Land Use Policy* **2022**, *114*, 105994. https://doi.org/10.1016/j.landusepol.2022.105994
35. Zheng, A.; Ba, R.; Jiang, W.; et al. Intelligent fire modeling in wildland-urban interface: A comprehensive review of current progress, challenges, and future perspectives. *J. Saf. Sci. Resil.* **2025**, *7*, 100252. https://doi.org/10.1016/j.jnlssr.2025.100252
36. Kuhn, R.L. A landscape of consciousness: Toward a taxonomy of explanations and implications. *Prog. Biophys. Mol. Biol.* **2024**, *190*, 28–169. https://doi.org/10.1016/j.pbiomolbio.2023.12.003
37. Parsch, C.; Wagner, B.; Engert, J.E.; et al. Forecasting deforestation and carbon loss across New Guinea using machine learning and cellular automata. *Sci. Total Environ.* **2025**, *970*, 178864. https://doi.org/10.1016/j.scitotenv.2025.178864
38. Kidmose, B. A review of smart vehicles in smart cities: Dangers, impacts, and the threat landscape. *Veh. Commun.* **2024**, *51*, 100871. https://doi.org/10.1016/j.vehcom.2024.100871
39. Yang, H.; Xu, W.; Yu, J.; et al. Exploring the impact of changing landscape patterns on ecological quality in different cities: A comparative study among three megacities in eastern and western China. *Ecol. Inform.* **2023**, *77*, 102255. https://doi.org/10.1016/j.ecoinf.2023.102255
40. Bettinger, P.; Sandoval, S.; Merry, K.; et al. Approaches for simulating alternative futures of complex forested landscapes: A review. *Environ. Dev.* **2025**, *56*, 101285. https://doi.org/10.1016/j.envdev.2025.101285
41. Zou, L.; Chen, J.; Wang, Y.; et al. Simulating tropical forest change using a cellular automata-agent based model. *Ecol. Model.* **2025**, *509*, 111256. https://doi.org/10.1016/j.ecolmodel.2025.111256
42. USGS (United States Geological Survey). *Earth Explorer Platform, 2025*; U.S. Geological Survey (USGS): Reston, VA, USA, 2025. Official Website: https://earthexplorer.usgs.gov/
43. Sorsa, Y.; Abate, B.; Arba, Y. Analyzing historical land use land cover changes using machine learning approach integrated with geospatial techniques in Omo Gibe River Basin, Ethiopia. *Environ. Chall.* **2025**, *20*, 101296. https://doi.org/10.1016/j.envc.2025.101296
44. Aszkowski, P.; Ptak, B.; Kraft, M.; et al. Deepness: Deep neural remote sensing plugin for QGIS. *SoftwareX* **2023**, *23*, 101495. https://doi.org/10.1016/j.softx.2023.101495
45. Jakimow, B.; Janz, A.; Thiel, F.; et al. EnMAP-Box: Imaging spectroscopy in QGIS. *SoftwareX* **2023**, *23*, 101507. https://doi.org/10.1016/j.softx.2023.101507
46. Mafiana, C.F.; Izunobi, J.U.; Iduseri, E.O.; et al. Sustainable development goals and effects of Land-Use–Land-Cover (LULC) changes on vegetation using Kubanni River Basin, Zaria, Nigeria as a case-in-point. *Ecohydrol. Hydrobiol.* **2025**, *25*, 100694. https://doi.org/10.1016/j.ecohyd.2025.100694
47. Rodríguez-Ortega, J.; Tabik, S.; Benhammou, Y.; et al. Land use and land cover fraction estimation for Sentinel-2 RGB images: A new LULC mapping task. *Remote Sens. Appl. Soc. Environ.* **2025**, *39*, 101626. https://doi.org/10.1016/j.rsase.2025.101626
48. López-Ballesteros, A.; Srinivasan, R.; Senent-Aparicio, J. Introducing MapSWAT: An open source QGIS plugin integrated with google earth engine for efficiently generating ready-to-use SWAT+ input maps. *Environ. Model. Softw.* **2024**, *179*, 106108. https://doi.org/10.1016/j.envsoft.2024.106108
49. Facun, L.P.; Maria, M.Y.S.; Ducao, R.; et al. QGIS Shoreline Change Analysis Tool (QSCAT): A fast, open-source shoreline change analysis plugin for QGIS. *Environ. Model. Softw.* **2025**, *184*, 106263. https://doi.org/10.1016/j.envsoft.2024.106263
50. Julien, A.; Giguet-Covex, C.; Messager, E.; et al. Performance of the REVEALS model to reconstruct present mountain vegetation cover in the North-Western Alps: A model evaluation for past land cover reconstruction. *Quat. Sci. Rev.* **2025**, *349*, 109089. https://doi.org/10.1016/j.quascirev.2024.109089
51. Benitez, F.L.; Mena, C.F.; Laso, F.; et al. Trajectories of farming systems reshape land use/land cover dynamics in the agricultural

zones of the Galapagos Islands. *Agric. Syst.* **2026**, *231*, 104506. http://dx.doi.org/10.1016/j.agsy.2025.104506

52. Babitha, A.; Andrushia, A.D.; Anand, N.; et al. Land use and land cover change detection from multisource satellite imagery—A hybrid convolutional neural network approach. *Eng. Appl. Artif. Intell.* **2025**, *161*, 112187. https://doi.org/10.1016/j.engappai.2025.112187
53. Mupepi, O.; Marambanyika, T.; Matsa, M.M.; et al. Land use and land cover changes in sub-catchments of Zimbabwe and their implications on wetland and catchment soil water conditions. *Phys. Chem. Earth* **2025**, *141*, 104081. https://doi.org/10.1016/j.pce.2025.104081
54. Korcelski, C.; Neckel, A.; Bodah, B.W.; et al. Terrestrial nanoparticles and geospatial optics: Implications for environmental impact from anthropogenic contaminants in the Caribbean region. *Sci. Total Environ.* **2025**, *963*, 178503. https://doi.org/10.1016/j.scitotenv.2025.178503
55. Khan, A.; Sudheer, M. Machine learning-based monitoring and modeling for spatio-temporal urban growth of Islamabad. *Egypt. J. Remote Sens. Space Sci.* **2022**, *25*, 541–550. https://doi.org/10.1016/j.ejrs.2022.03.012
56. Shomope, I.; Tawalbeh, M.; Al-Othman, A.; et al. Predicting biohydrogen production from dark fermentation of organic waste biomass using Multilayer Perceptron Artificial Neural Network (MLP–ANN). *Comput. Chem. Eng.* **2025**, *192*, 108900. https://doi.org/10.1016/j.compchemeng.2024.108900
57. Blissag, B.; Yebdri, D.; Kessar, C. Spatiotemporal change analysis of LULC using remote sensing and CA-ANN approach in the Hodna basin, NE of Algeria. *Phys. Chem. Earth* **2024**, *133*, 103535. https://doi.org/10.1016/j.pce.2023.103535
58. Ali, M.A.; Jamal, S.; Wahid, N.; et al. Leveraging CA-ANN modelling for SDGs alignment: Previse future land use patterns and their influence on Mirik Lake of sub-Himalayan region. *World Dev. Sustain.* **2025**, *6*, 100218. https://doi.org/10.1016/j.wds.2025.100218
59. Foody, G.M. Explaining the unsuitability of the kappa coefficient in the assessment and comparison of the accuracy of thematic maps obtained by image classification. *Remote Sens. Environ.* **2020**, *239*, 111630. https://doi.org/10.1016/j.rse.2019.111630
60. Ismaeel, W.A.; Kumar, J.S. An approach for built-up area extraction using different indices and deep neural network (DNN) model. *Infrared Phys. Technol.* **2024**, *142*, 105558. https://doi.org/10.1016/j.infrared.2024.105558
61. Tola, B.; Deyassa, G. A modeling approach for evaluating and predicting the impacts of land use land cover changes on groundwater recharge in Walga Watershed, Upper Omo Basin, Central Ethiopia. *J. Hydrol. Reg. Stud.* **2024**, *51*, 101659. https://doi.org/10.1016/j.ejrh.2024.101659
62. Zhang, R.; Wen, L.; Jin, Y.; et al. Synergistic impacts of carbon emission trading policy and innovative city pilot policy on urban land green use efficiency in China. *Sustain. Cities Soc.* **2024**, *118*, 105955. https://doi.org/10.1016/j.scs.2024.105955
63. Dinh, T.; Tran, D.; Dobešová, Z.; et al. An efficient fusion-based deep learning framework for land use and land cover image clustering. *Eng. Appl. Artif. Intell.* **2025**, *161*, 112061. https://doi.org/10.1016/j.engappai.2025.112061
64. Maze, M.; Attaher, S.; Taqi, M.O.; et al. Enhanced agricultural land use/land cover classification in the Nile Delta using Sentinel-1 and Sentinel-2 data and machine learning. *ISPRS J. Photogramm. Remote Sens.* **2025**, *229*, 239–253. https://doi.org/10.1016/j.isprsjprs.2025.08.019
65. Zhou, Y.; Ferdinand, M.S.; Van Wesemael, J.; et al. A framework for mapping conservation agricultural fields using optical and radar time series imagery. *Remote Sens. Environ.* **2025**, *328*, 114858. https://doi.org/10.1016/j.rse.2025.114858
66. Cáceres, N.R.; Garcia-Martinez, A.; De Cózar, J.C.G. Use of GIS and BIM tools in determining the life cycle impact of urban systems. Case study: Residential buildings which apply the Eco-Efficiency Matrix in the city of Quito, Ecuador. *J. Clean. Prod.* **2022**, *383*, 135485. https://doi.org/10.1016/j.jclepro.2022.135485
67. Moravej, M.; Kenway, S.; Renouf, M.; et al. Population and land cover projections under greyfield development: Implications for densification, urban forest, water performance, and heat. *Cities*, **2025**, *167*, 106323. https://doi.org/10.1016/j.cities.2025.106323
68. Qi, L.; Najam, H.; Oskenbayev, Y.; et al. Impact of rapid urban construction land expansion on spatial inequalities of ecosystem health in China: Evidence from national, economic regional, and urban agglomeration perspectives. *Ecol. Indic.* **2025**, *172*, 113196. https://doi.org/10.1016/j.ecolind.2025.113196
69. Grahani, B.P.; Flores, F.P.; Prasetyo, Y.T.; et al. Assessing factors influencing flood preparedness among Jakarta residents: A multilayer perceptron artificial neural network based on protection motivation theory. *Environ. Dev.* **2026**, *57*, 101358. https://doi.org/10.1016/j.envdev.2025.101358
70. Jabali, O. Urban infrastructure under occupation: Reimagining sustainability in Beita municipality. *City Environ. Interact.* **2025**, *28*, 100250. https://doi.org/10.1016/j.cacint.2025.100250
71. Lima, K.C.O.; Ferraz, L.L.; Santana, G.M.; et al. Integrated use of the analytical hierarchy process method for mapping areas susceptible to flooding in the urban area in a city in southwest Bahia, Brazil. *J. S. Am. Earth Sci.* **2025**, *167*, 105778. https://doi.org/10.1016/j.jsames.2025.105778
72. Baidoo, R.; Arko-Adjei, A.; Poku-Boansi, M.; et al. Land use and land cover changes implications on biodiversity in the Owabi catchment of Atwima Nwabiagya North District, Ghana. *Heliyon* **2023**, *9*, e15238. https://doi.org/10.1016/j.heliyon.2023.e15238